The nature of assembly bias - I. Clues from a ΛCDM cosmology

Ivan Lacerna[1] and Nelson Padilla[1]

[1]*Departamento de Astronomía y Astrofísica, Pontificia Universidad Católica de Chile, V. Mackenna 4860, Santiago 22, Chile.*

ABSTRACT

We present a new proxy for the overdensity peak height for which the large-scale clustering of haloes of a given mass does *not* vary significantly with the assembly history. The peak height, usually taken to be well represented by the virial mass, can instead be approximated by the mass inside spheres of different radii, which in some cases can be larger than the virial radius and therefore include mass outside the individual host halo. The sphere radii are defined as $r = a\ \delta_t + b\ \log_{10}\left(M_{vir}/M_{nl}\right)$, where δ_t is the age relative to the typical age of galaxies hosted by haloes with virial mass M_{vir}, M_{nl} is the non-linear mass, and $a = 0.2$ and $b = -0.02$ are the free parameters adjusted to trace the assembly bias effect. Note that r depends on both halo mass and age. In this new approach, some of the objects which were initially considered low-mass peaks (i.e. which had low virial masses) belong to regions with higher overdensities. At large scales, i.e. in the two-halo regime, this model properly recovers the simple prescription where the bias responds to the height of the mass peak alone, in contrast to the usual definition (virial mass) that shows a strong dependence on additional halo properties such as formation time. The dependence on the age in the one-halo term is also remarkably reduced with the new definition. The population of galaxies whose "peak height" changes with this new definition consists mainly of old stellar populations and are preferentially hosted by low-mass haloes located near more massive objects. The latter is in agreement with recent results which indicate that old, low-mass haloes would suffer truncation of mass accretion by nearby larger haloes or simply due to the high density of their surroundings, thus showing an assembly bias effect. The change in mass is small enough that the Sheth et al. (2001) mass function is still a good fit to the resulting distribution of new masses.

Key words: cosmology: large-scale structure of Universe - cosmology: theory - cosmology: dark matter - galaxies: statistics - galaxies: formation

1 INTRODUCTION

Many recent models of galaxy formation assume that galaxy properties are determined by the haloes in which they form and not by the surrounding larger-scale environment (e.g. Kauffmann et al. 1997; Berlind et al. 2003; Yang et al. 2003; Baugh et al. 2005). In this picture, the galaxy population in a halo of a given mass is independent of where the halo is located. This is justified by the standard description of structure formation, namely the extended Press-Schechter theory (EPS, Bond et al. 1991; Lacey & Cole 1993; Mo & White 1996), which was in turn based on both linear growth theory of density perturbations of an initial Gaussian random fluctuation field (Press & Schechter 1974) and the non-linear spherical collapse model. Furthermore, simulation re-

sults as recent as Percival et al. (2003) indicated that the halo clustering should only depend on the mass.[1]

However, a few years ago, it was shown that galaxy properties such as the star formation rate (Gomez et al. 2003; Balogh et al. 2004; Ceccarelli et al. 2008; and Padilla, Lambas, Gonzalez 2010 in observations; Gonzalez & Padilla 2009 in numerical simulations) and colours (Gonzalez & Padilla 2009) depend on the large-scale structure. Gomez et al. (2003) found that, for a sample of galaxies in groups and clusters from the Sloan Digital Sky Survey (SDSS), the star formation rate decreases, compared with the field population, starting at ~ 4 virial radii to-

---

[1] Although these authors mention that a systematic difference between the clustering of the set of all haloes of a given mass and any of their subsamples could be hidden within the noise at a level below 20 per cent in the bias.

ward the cluster centre. Gonzalez & Padilla (2009) used a semi-analytic model of galaxy formation and found that the fraction of red galaxies diminishes for galaxies farther away from clusters (or closer to voids) in environments with the same local density. These results support the view that galaxy populations also depend on the larger-scale environment, both in models and observations.

Regarding the fact that haloes of the same mass should essentially exhibit the same properties, Gao et al. (2005, hereafter G05) measured that the large-scale clustering of haloes of a given mass depends strongly on the formation time, for halo masses $M \leqslant 6 \times 10^{12}$ h^{-1} $M_{\odot}$. This study, based on N-body simulations, showed that haloes assembled at high redshift are more strongly correlated than those of the same mass that assembled recently. This effect, which is not expected from the excursion set theory, was termed "assembly bias," which consists in that the large-scale clustering of haloes of a given mass varies significantly with their assembly history (Gao & White 2007).

On the observational side of the assembly bias, Wang et al. (2008) found that groups selected from the SDSS with red central galaxies are more strongly clustered than groups of the same mass but with blue centrals, being this effect much more important for less massive groups. In addition to the clustering amplitude, Zapata et al. (2009) found that galaxy groups of similar mass and different assembly histories show differences in their galaxy population, for example in the fraction of red galaxies. Furthermore, Cooper et al. (2010) studied the relationship between the local environment and properties of galaxies in the red sequence. After removing the dependence of the average overdensity on colour and stellar mass, they still found a strong dependence on the luminosity-weighted stellar age. Galaxies with older stellar populations occupy regions of higher overdensities compared to younger galaxies of similar colours or stellar masses. The latter results show that the concept of assembly bias could be applicable to galaxies in addition to dark matter haloes, and would then affect the physics of galaxy formation.

Other halo properties such as concentration, number of subhaloes, subhalo mass function, shape, halo spin, major merger rate, triaxiality, shape of the velocity ellipsoid, and velocity anisotropy at a given mass show an assembly-type bias effect in cosmological N-body simulations (Wechsler et al. 2006; Zhu et al. 2006; Croton et al. 2007; Bett et al. 2007; Gao & White 2007; Hester & Tasitsiomi 2010; Faltenbacher & White 2010).

The reasons for this assembly bias are not yet fully understood. EPS assumes no such environmental dependence. At a fixed mass, the Markovian nature of the random walk trajectories of perturbations smoothed at higher resolution, which characterise a halo, is assumed to be independent of the environment encoded in random walks at lower resolution. Thus, halo properties should not be related with the external environment in haloes of equal mass. These random walks are obtained using a top-hat Fourier-space window function to smooth (or to average) the density fluctuations; this filter in k-space allows to obtain an analytic expression of the halo mass function that is equal to the Press-Schechter formula. There have been attempts to modify this window function to consider an environmental dependence. Zentner (2007) combined a Gaussian window function and a vari-

able height of the barrier for collapsed objects, but found an opposite trend for the assembly bias at low masses.

Furthermore, correlations between halo parameters do not simply show the same clustering behaviour. Bett et al. (2007) found that both the most nearly spherical haloes and those with highest spins are more strongly clustered than the average. However, this fact contradicts the correlation between spin and shape, where more spherical haloes have on average a slightly lower spin parameter. Also, for example, the work by Croton et al. (2007) showed that there are aspects of the assembly history which are not encoded in halo concentration or formation redshift and which correlate with the large-scale environment. One possible explanation was suggested by Dalal et al. (2008). They claim that the halo assembly bias is related to the peak curvature of Gaussian random fields in high-mass haloes, whereas at the low-mass regime the bias arises from a subpopulation of low-mass haloes whose mass accretion has ceased. These haloes could have been ejected out of nearby massive haloes (Ludlow et al. 2009). Wang et al. (2009) found that these ejected low-mass subhaloes have earlier assembly times and a much higher bias parameter than normal (not ejected) haloes of the same mass, so that they contribute to the assembly bias. However, they also found that the assembly bias is not dominated by this population, indicating that effects of the large-scale environment on "normal" haloes is the main source for this bias.

Despite the fact that halo mass continues to be the most important parameter to determine the galaxy properties, it is relevant to study the assembly bias to gain further insights on the development of the Large-Scale Structure. This is particularly significant when galaxies are used to constrain cosmological parameters, as shown by Wu et al. (2008) in their study of the effects of halo assembly bias on galaxy cluster surveys. They used the halo concentration to find that upcoming photometric projects such as the Dark Energy Survey (DES) and the Large Synoptic Survey Telescope (LSST) can infer significantly biased cosmological parameters from the observed clustering amplitude of galaxy clusters if the assembly bias is not taken into account.

Hester & Tasitsiomi (2010, hereafter HT10) found an assembly-type bias in that the rate of major mergers of haloes of a given mass changes with the local environment. They proposed a dynamical explanation for this effect, particularly for high densities, based on both tidal stripping, responsible for the decrease in the major merger rate of galaxy-like haloes, and interactions between bound haloes in the outskirts of groups, which are related with the increase in the merger rate in group-like haloes. This plausible explanation applies on scales of out to ~ 250 kpc.

We suggest that, if the initial peak did not collapse completely onto haloes, their mass will not be an appropriate proxy for the peak height. They will present old ages, which would not be the case if the peak finished its collapse onto the halo (it would look younger dynamically). Therefore, the scale out to which we need to extend the inclusion of mass for the peaks could be as large as or even larger than the scale proposed by HT10 since, at low z, the initial overdensity may be still spread in larger areas around the current collapsed halo. Wang et al. (2007) mention a similar idea in that old, low-mass haloes were part of higher peaks in the initial density field than what is revealed by

their present-day virial mass. By means of a semi-analytic model, we will show that, at the present time, the assembly bias may well be related with the infall region of a halo for scales 80 kpc $<$ r$/h^{-1}$ $<$ 1.5 Mpc, a range where the one-halo clustering amplitude between populations of the same mass but different ages differs strongly (see Section 3.1).

The aim of this work is to understand the origin of the assembly bias and its role in the development of the large-scale structure and on the galaxy population, beyond the halo mass dependence. In order to reach this goal, we will study this effect on the semi-analytic galaxies of the Lagos, Cora, & Padilla (2008) model. This will allow us to compare our results with those obtained from observational data in future work, so as to provide another test for the ΛCDM model of the Universe. Also, we will show that it is fundamental to include the global effect from large scales on the peak height estimate. The results obtained with this proxy of the peak height will be compared with those obtained from the virial mass of host haloes by means of the spatial two-point correlation function and infall velocity profiles for galaxy samples of different relative ages. This new definition of an overdensity peak height will not be subject to the assembly bias seen at large separations, thus objects of the same mass but different ages will show essentially the same clustering in the two-halo regime. Given that the assembly bias has also been detected separating samples according to several other parameters than the halo age, in subsequent papers we will also investigate its prevalence when studying galaxies and haloes of different concentrations, number of satellites, sphericity, and whether our proposed explanation for the assembly bias also responds when using observational data.

The outline of this paper is as follows. In Section 2, we introduce our simulation. We then perform the statistics of density fields for the simulation in Section 3 to compare our results with those from other authors that show the assembly bias effect. The redefinition of the overdensity peak height by using the two-point correlation function and the infall velocity profile is developed in Section 4. The nature of the objects that are being considered with this redefinition are shown in Section 5. Finally, we discuss our results in Section 6. The cosmology used here is $\Omega_{tot} = 1$, $\Omega_m = 0.28$, $\Omega_\Lambda = 0.72$, $\sigma_8 = 0.9$, $h = 0.72$, unless otherwise indicated.

2 DATA

We use the SAG2 model by Lagos, Cora, & Padilla (2008; see also Lagos, Padilla, & Cora 2009), which combines a cosmological N-body simulation of the concordance ΛCDM universe and a semi-analytic model of galaxy formation. The numerical simulation consists of a periodic box of 60 h^{-1} Mpc on a side that contains 256^3 dark matter particles with a mass resolution of $\sim 10^9$ h^{-1} M$_\odot$. The galaxy population in the semi-analytic model is generated using the merger histories of dark matter haloes. One of the main features of this model is the implementation of the Active Galactic Nuclei (AGN) feedback, which reduces star formation by quenching the gas cooling process, an important effect on massive haloes at low redshifts.

One of the most important parameters throughout this work is the age. We will use it to study the assembly bias

effect for galaxies of a wide range of luminosities and, also, for dark matter haloes of a wide range in mass.

For galaxies, we will use the mass-weighted stellar age or, simply, stellar age defined as

$$t = t_0 - \frac{\sum t_i \Delta t_i \dot{M}_{star}}{\sum \Delta t_i \dot{M}_{star}}, \qquad (1)$$

where t_0 is the age of the Universe today, t_i is the time corresponding to the ith output of the simulation, and $\dot{M}_{star}$ is the star formation rate calculated using the stellar mass ΔM_{star} accreted in a time step Δt_i. We use this parameter, the stellar age, as it can be directly obtained from observational data (Kauffmann et al. 2003; Gallazzi et al. 2005).

On the other hand, the formation redshift of a dark matter (DM) halo is defined as the redshift when it assembled 50 per cent of its final mass at $z = 0$. It is important to mention that the assembly bias has been detected by using this definition of age for DM haloes, and thus it will be used in this work. There are other definitions that show a weaker or absent dependence of halo clustering on the halo formation time, as was shown by Li et al. (2008).

2.1 Age parameter

To study the assembly bias, which consists in that old haloes have a higher clustering than young haloes of the same mass, it is not convenient to work directly with the stellar or halo formation age because they correlate with the mass. For example, massive dark matter haloes have, on average, older stellar populations (Figure 1). We need a definition of age which is independent of the mass. This is very important if we want to study galaxies in haloes of a wide range of masses. For example, age maps could show old objects in regions inhabited only by massive haloes. Motivated by this problem, the first step is to find a proxy for a non-mass-dependent age. One way to do this consists in using ages relative to the median stellar age as a function of the host DM halo mass. We define the δ_t dimensionless parameter,

$$\delta_{t_i} = \frac{t_i - \langle t(M) \rangle}{\sigma_t(M)}, \qquad (2)$$

where, for the ith galaxy, t_i is its stellar age, $\langle t(M) \rangle$ is the median stellar age as a function of host halo mass (red squares connected by the solid line in Fig. 1), with M being the virial mass, and $\sigma_t(M)$ the dispersion around the median in units of time (error bars in Fig. 1). In the case of DM haloes, t_i is the formation redshift. This definition implies that objects with positive (negative) values of δ_t lie above (below) the median stellar age or formation time for a population of a given mass. Then, positive values of δ_t correspond to older objects, whereas negative values of δ_t are related to younger objects. The histogram in Figure 2 shows the distribution of the δ_t parameter for galaxies in different mass bins. The shape of the distribution of δ_t is similar among them. Also, the median host halo mass for $\delta_t < 0$ and $\delta_t > 0$ is similar, $< M > \sim 1.7 \times 10^{10}$ h^{-1} M$_\odot$, confirming that this parameter is independent of the DM halo mass.
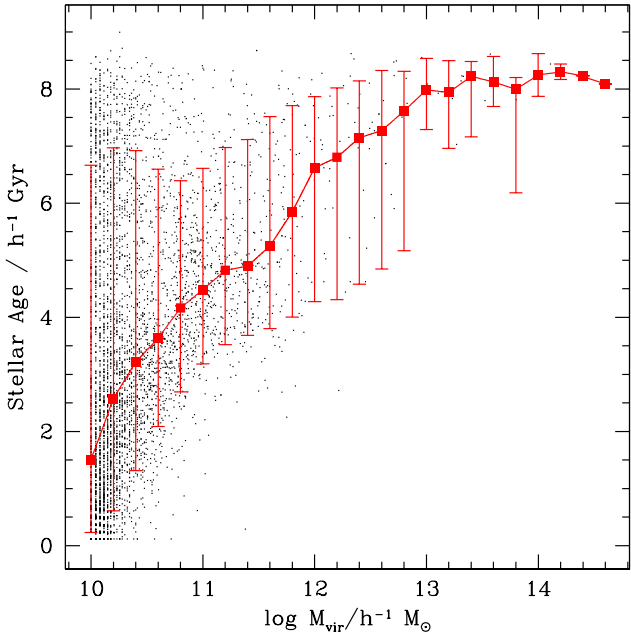
Figure 1. Stellar age as a function of the virial mass (logarithms are base 10 throughout) for the galaxies in the simulation. Due to the large number of available galaxies, only 5,000 of them, randomly chosen, are plotted as points. Red squares are the medians for each mass bin. Error bars correspond to the 10 and 90 percentiles of the stellar age distribution. The median stellar population of low-mass dark matter haloes is younger than that of the massive DM haloes.
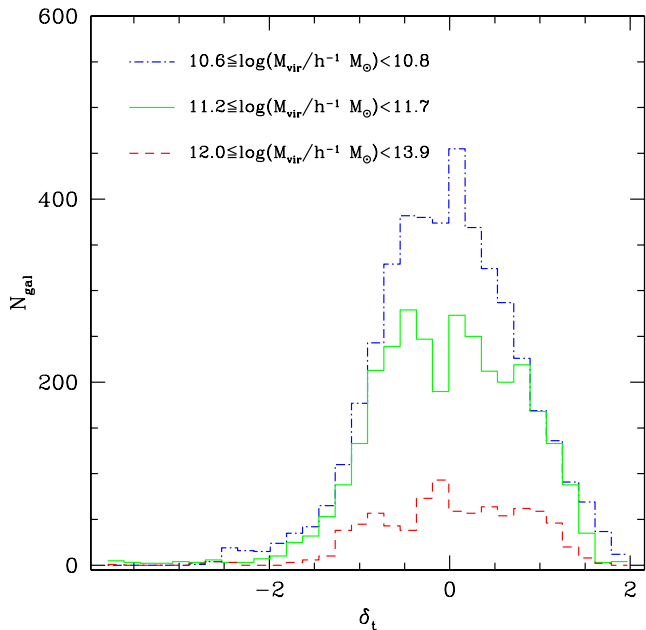

Figure 2. Histograms of the δ_t parameter for the different mass ranges indicated in the figure key. The three distributions are similar and cover the full range of δ_t. This parameter is independent of the DM halo mass.

3   STATISTICS OF DENSITY FIELDS

In this section we present the two-point correlation function which allows us to calculate the clustering of haloes and galaxies, measured directly from the simulation and from theoretical expressions for the power spectrum.

3.1   The two-point correlation function

The correlation function, $\xi(r)$, is a useful quantitative measure of the spatial clustering. It gives the excess probability for finding pairs of particles at a given separation relative to a Poisson distribution. The distribution for two points separated by a distance r, with respective volume elements dV_1 and dV_2, is given by

$$dP = n^2[1 + \xi(r)]dV_1 dV_2, \tag{3}$$

where n is the average number density of points.

In practice the estimator used, particularly for numerical simulations with periodic boundary conditions, is

$$DD(r) = RR(r)[1 + \xi(r)],$$

and then

$$\xi(r) = \frac{DD(r)}{RR(r)} - 1. \tag{4}$$

Here, $DD(r)$ represents the frequency of the data pairs, whereas $RR(r)$ corresponds to the frequency of random pairs, defined as

$$RR(r) = N_{sel} N_{tot} \frac{V(r)}{V_{box}}, \tag{5}$$

where N_{sel} is the number of selected objects in a given sample, N_{tot} is the total number of objects, and $V(r)$ is the volume in a shell at distance r which is normalised by the volume of the box V_{box} in the simulation. In the case of an auto-correlation function, $N_{tot} = N_{sel}$.

The cross-correlation function estimates the clustering amplitude between two different data sets. We will calculate this function for a selected sample against all the available objects in the simulation because it will have a higher signal than the correlation between the same selected elements, i.e. the autocorrelation function (e.g. Bornancini et al. 2006).

3.1.1   Cross-correlation function for haloes

In order to test whether our simulation is able to reproduce the observed signal of assembly bias at large scales found by other authors, Figure 3 shows the spatial cross-correlation function for haloes of different formation times and a given mass against the full population of haloes in the simulation, at $z = 0$ (top panels). The two ranges of masses shown in the figure are the same as those used by G05 in two panels of their Fig. 2 which exhibit the assembly bias effect. The result for the 20% oldest δ_t haloes in each mass range is shown as dot-dashed red lines, while that for the 20% youngest haloes is shown as dotted blue lines. Note that in the panels of their Figure 2, G05 show the autocorrelation function of haloes.
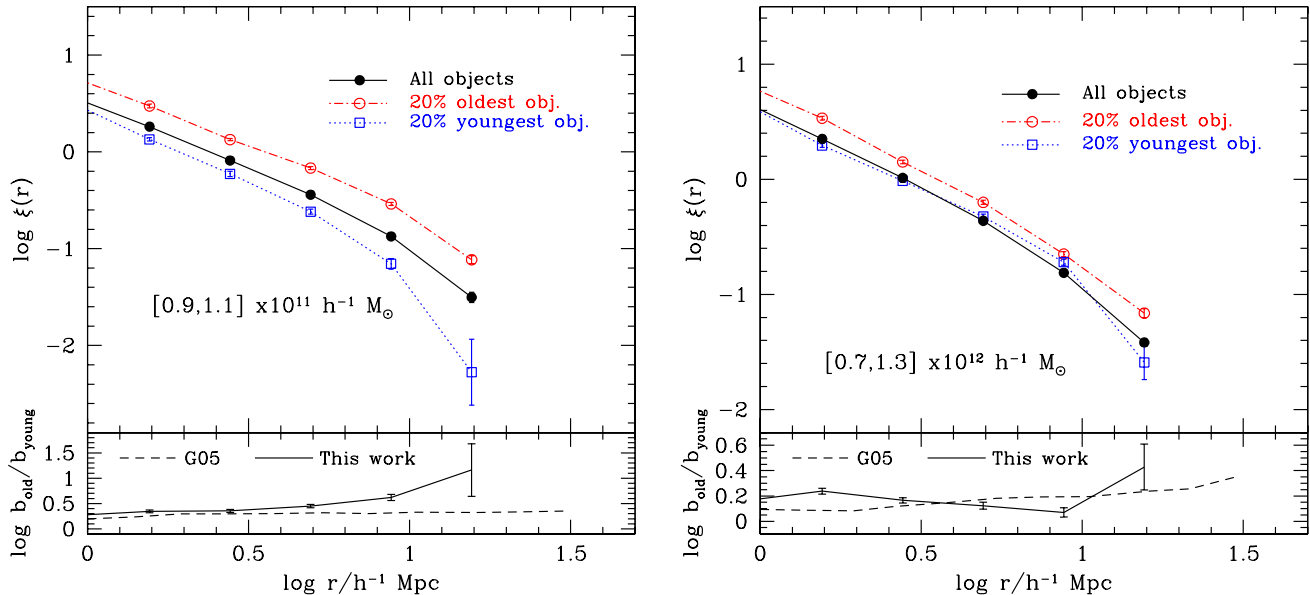
Figure 3. *Main panels (top):* Two-point cross-correlation function for haloes from our simulation for two different ranges of mass (left and right panels). The old population is represented as dot-dashed red lines, whereas the young one appears as dotted blue lines (the full population of haloes are shown as solid black lines). Error bars were calculated using the jackknife method. *Lower panels:* ratio between the bias of old and young objects in our simulation (solid lines) and in G05 (dashed lines). At large scales, both simulations show a higher clustering for the old haloes with respect to the young ones with a remarkable difference for the lowest mass bin (left-hand panel). Our simulation is able to measure the assembly bias effect with a high statistical significance.

To compare their estimates of assembly bias with ours, we consider the expression found in Mo & White (1996) for the bias of a given halo sample, b_H, on large scales,

$$\xi_{HH}(r, M) = b_H^2(M)\xi_{mm}(r), \quad (6)$$

where ξ_{HH} is the autocorrelation function for haloes and ξ_{mm} is that for the underlying matter, which assumes that the halo density field is proportional to the matter density field times the bias parameter. If the population of haloes is separated into old and young subpopulations, the ratio between the bias of these samples is, in the G05 case,

$$\frac{b_{H,old}}{b_{H,young}} = \sqrt{\frac{\xi_{HH,old}}{\xi_{HH,young}}}. \quad (7)$$

In our case, we calculate the cross-correlation function as

$$\xi_{HH'}(r, M) = b_H(M)b_{H'}(M)\xi_{mm}(r). \quad (8)$$

The subscript H refers to the selected haloes in a mass bin, whereas H' represents all the haloes in our simulation. Then,

$$\frac{b_{H,old}}{b_{H,young}} = \frac{\xi_{HH',old}}{\xi_{HH',young}}. \quad (9)$$

These ratios are shown as dashed and solid lines in the lower

panels of Figure 3 for the G05 and our simulation, respectively.[2]

As can be seen from these panels, both simulations show a higher clustering for the old population than that for the young one, and it can also be seen that our simulation can reproduce the assembly bias effect with an appropriate statistical significance, particularly for low-mass haloes.

3.1.2 Galaxy cross-correlation functions

The top row of Figure 4 shows the spatial cross-correlation function between galaxy samples of different relative ages δ_t but equal host halo masses, and the full population of galaxies in our simulation ($\sim$ 63,000 objects). Using δ_t, we find an assembly bias effect in our galaxies where the old population (red filled triangles and open circles) shows a higher clustering than the young population (blue open and filled squares), being this effect much stronger for the low-mass regime. The lower box in each panel shows the ratios between the correlation function of the oldest population (red triangles) and the total population, and between the youngest population (filled blue squares) and the total one, as dot-dashed red and dotted blue lines, respectively. The error of the ratio between $\xi(r)$ for the oldest and youngest objects is shown as a shaded region around the value that would be obtained if both correlation functions were the same (ratio equal to unity).

As can be seen from the lowest-mass bin (top left

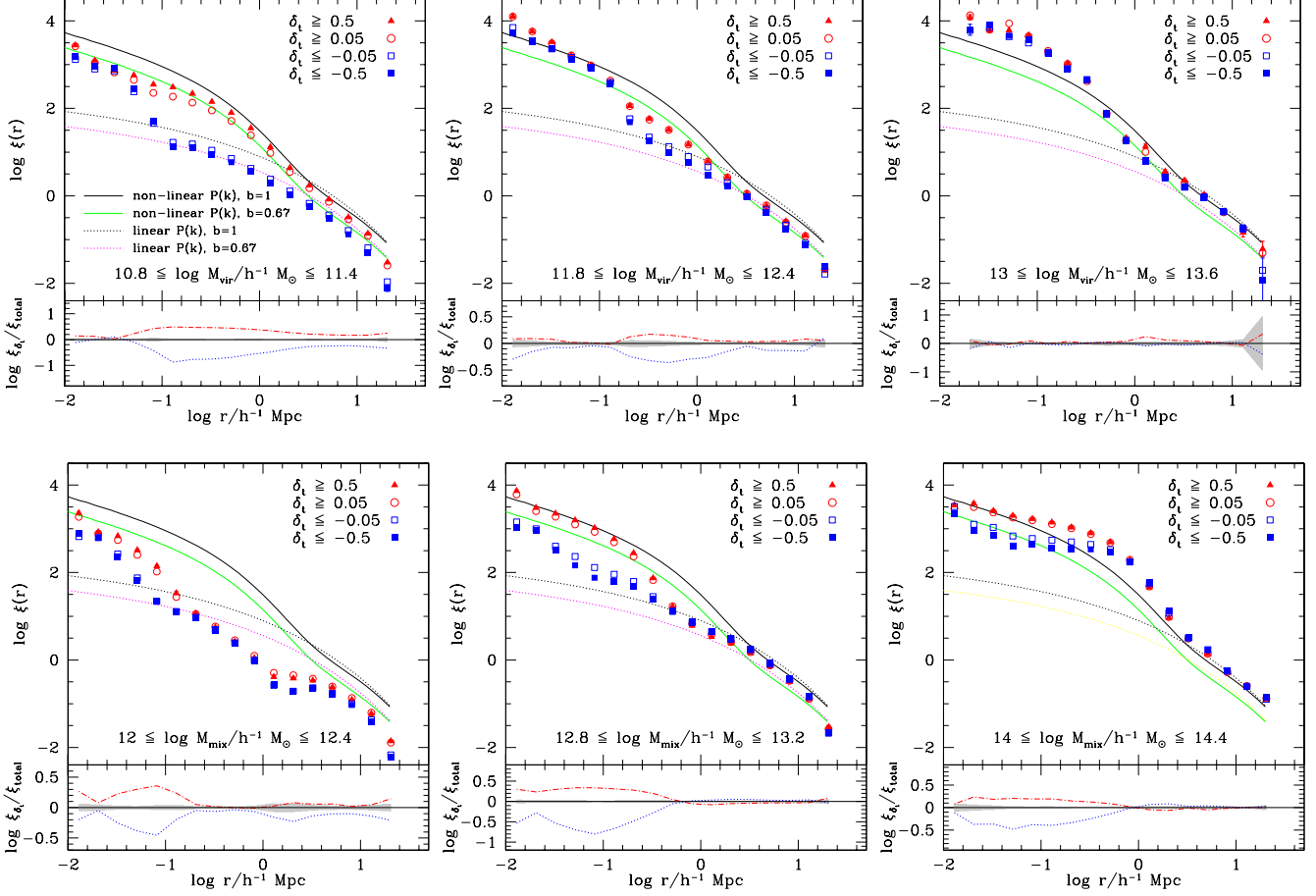[2] The cosmology in G05 was adjusted to that used in this paper.

Figure 4. Correlation functions for the different mass bins indicated in each panel. Old and young galaxies are shown in red and blue symbols, respectively. The figure key shows the ranges of δ_t corresponding to the different symbols. Error bars were calculated using the jackknife method. The lines repeated in each top box are obtained from the non-linear and linear power spectra, $P(k)$ (labels indicated in the top left panel). See details in Section 3.2). The lower box in each panel corresponds to the ratio between the correlation function of the oldest population (red triangles) and the total population of the selected sample and, also, between the youngest population (filled blue squares) and the total one (dot-dashed red and dotted blue lines, respectively). The error of the ratio between the $\xi(r)$ of the oldest and youngest objects is shown as a shaded region around the unit ratio. *Top row*: The age definition using the virial mass of the host halo. Notice the strong difference of almost two orders of magnitude between the old and young populations at $r \sim 150\ h^{-1}$ kpc for the lowest mass bin. *Bottom row*: Galaxies are selected according to a tentative new mass measurement, M_{mix} (see Section 4.1).

panel), the amplitude of clustering is higher for the old population than the young one, particularly for scales 80 kpc $< \mathrm{r}/h^{-1} < 1.5$ Mpc (one-halo term). This could indicate that their density profiles are different, probably those of the young population being dynamically less internally evolved. The strong difference in clustering at distances beyond $1\ h^{-1}$ Mpc may imply that if the mass in the vicinities (surrounding areas or the infall region) of haloes were taken into account, it would show no dependence on age. In other words, as the virial mass of haloes is not good enough as an overdensity peak height estimator in the simple EPS picture, this alternative could provide a better estimator for this peak height. HT10 detected an assembly-type bias for the dark matter halo major merger rate using the Millennium Simulation (Springel et al. 2005), and proposed a physical mechanism for this effect that, as was mentioned above, extends out to ~ 250 kpc. Owing to the result seen in the top row of Figure 4, it is possible that to explain the assembly bias one would need to characterise the peak with mass on scales larger than the virial radius (see Section 4), extend-

ing the local definition of peak from within a halo to larger scales usually regarded as part of the global environment.

Additionally, recent studies have suggested that a population of subhaloes that were expelled from larger haloes located beyond three times the virial radius of the main halo could explain the age dependence of the clustering in the low-mass regime (Dalal et al. 2008; Ludlow et al. 2009). Although Wang et al. (2009) found that these low-mass haloes are not the main source for the assembly bias, they claim that environmental effects at large scales have a very important role on this issue. In this case, the mass of the expelled subhaloes are bad indicators of their peak height, which could be better represented by the higher mass of a larger halo.

Note that our results reproduce those found by previous authors where the dependence of the clustering on the assembly history is only detected in low-mass haloes. This indicates that the peak may include matter around haloes to distances that depend on both halo mass and age.

3.2 Theoretical estimates of $\xi(r)$

The statistical properties of the density fluctuation field can be represented by its power spectrum $P(k)$, or equivalently by its dimensionless power spectrum $\Delta^2(k)$,

$$\Delta^2(k) = \frac{k^3}{2\pi^2}P(k), \tag{10}$$

which measures the power per logarithmic unit bin in wavenumber k. This spectrum is a direct manifestation of the hierarchical growth of structures, where small-scale perturbations collapse first to grow and later form larger-scale perturbations which will collapse and form larger objects, in a non-linear process as time progresses. Directly related to this evolution are the abundance and clustering of galaxy systems and their variations as a function of mass and redshift. The Fourier transform of the power spectrum results in the matter correlation function

$$\xi_{mm}(r) = \int \Delta^2(k)\frac{\sin(kr)}{kr}\frac{dk}{k}. \tag{11}$$

The Smith et al. (2003) fitting model provides a good estimate for $\xi_{mm}(r)$ from the non-linear and the linear power spectra (Boylan-Kolchin et al. 2009). In order to do the comparison with the correlation function of galaxies in the simulation, we use Equations (8) and (11). The bias parameter b is estimated by using the fit proposed by Seljak & Warren (2004),

$$b_0(x = M/M_{nl}) = 0.53 + 0.39x^{0.45} + \frac{0.13}{40x + 1} + 5 \times 10^{-4}x^{1.5}, \tag{12}$$

with an accuracy on the bias-halo mass relation at the level of 3 per cent for $b < 1$. Here, M_{nl} refers to the non-linear mass, defined as the mass within a sphere for which the rms fluctuation amplitude of the linear field is 1.69 times the critical density of the Universe which corresponds to the gravitational collapse in the spherical collapse model (Gunn & Gott 1972). For our simulation, we find $M_{nl} \sim 2.4 \times 10^{13}\ h^{-1}\ M_\odot$.

The top boxes in each panel of Figure 4 show $\xi(r)$ as obtained from the non-linear power spectrum (solid black line) with $b = 1$; from the non-linear $P(k)$ (lower solid green line) with $b = 0.6733$ (corresponding to the average host halo mass); from the linear $P(k)$ with $b = 1$ (dotted black line); and from the linear $P(k)$ (lower dotted magenta line) with the bias factor for the average host halo mass. The biased $\xi(r)$ obtained from the non-linear $P(k)$ (lower solid green line) is expected to represent the correlation function without the assembly bias for the average host halo mass. The scale where the linear and non-linear power spectra start to diverge is around $\sim 1.5\ h^{-1}$ Mpc, and it is also out to where the correlation function shows the stronger difference in clustering between the old and young populations (top left panel of Figure 4). Therefore, we will start studying scales of this tentative size for estimating the height of the mass peak to see how it affects the galaxy clustering (Section 4.1). Later in this paper we will carry out a χ^2 search for this scale and its dependence on halo properties, since

the scale may introduce a large change in the resulting peak mass function.

4 REDEFINITION OF AN OVERDENSITY PEAK HEIGHT

We propose to extend the proxy for peak height to larger scales so that it does not show the assembly bias effect. The scale will include the mass of the peak which has already collapsed but also, in some cases, some of the mass that, due to global environmental effects, has not done so yet. This will be equivalent to a new definition of "halo." For each galaxy we will consider all the dark matter particles within a scale that will depend on the host halo mass and its age (see Section 4.3). The mass contained in this halo, together with the stellar age of each galaxy, will be used to study the large-scale bias.

Throughout this section, two different approaches that characterise the assembly bias, the two-point correlation function and the infall velocity profile, will be presented and later used to define the overdensity peak height. They will allow one to parametrise the scale which will trace the assembly bias at large scales.

4.1 Using $\xi(r)$ to determine the presence of an assembly-type bias

In a first attempt, we approximate the peak height for each galaxy considering all the DM particles inside a radius of 1.5 and 1.7 h^{-1} Mpc for old and young objects, respectively, motivated by the results of the previous section. We then repeat the same procedure described in Section 2.1. In this case, Equation (2) is applied using this new mass definition, M_{mix}. The results are shown in the bottom row of Figure 4. The left column shows the lower mass bin, whereas the most massive bin is shown in the right column. This peak height definition cannot fully trace the assembly bias at large scales for each mass bin, although it does a better job than the virial mass. Therefore, a redefinition of halo mass including larger scales than the virial radius could recover the simple prescription where the bias responds to the height of the mass peak alone. To achieve this goal, it thus seems necessary to consider influences beyond the virial radius, probably reaching the infall region of haloes.

It is important to point out that the redefinition of mass does not affect positions and hence only changes the relative age δ_t of a galaxy.

Since this tentative approximation may be overcorrected as the scale may depend on different parameters (e.g. mass, age), the next section will present an estimator for the size of the region to use for this new definition of peak height based also on the velocity profile of the infall region. Then, we will combine the constraints obtained from correlation functions and infall velocities to estimate a parametrised proxy for the peak height.

4.2 Using the Infall Velocity to determine the presence of an assembly-type bias

The infall velocity profile v_{inf} around galaxies is another statistic which is sensitive to the assembly bias. The v_{inf}
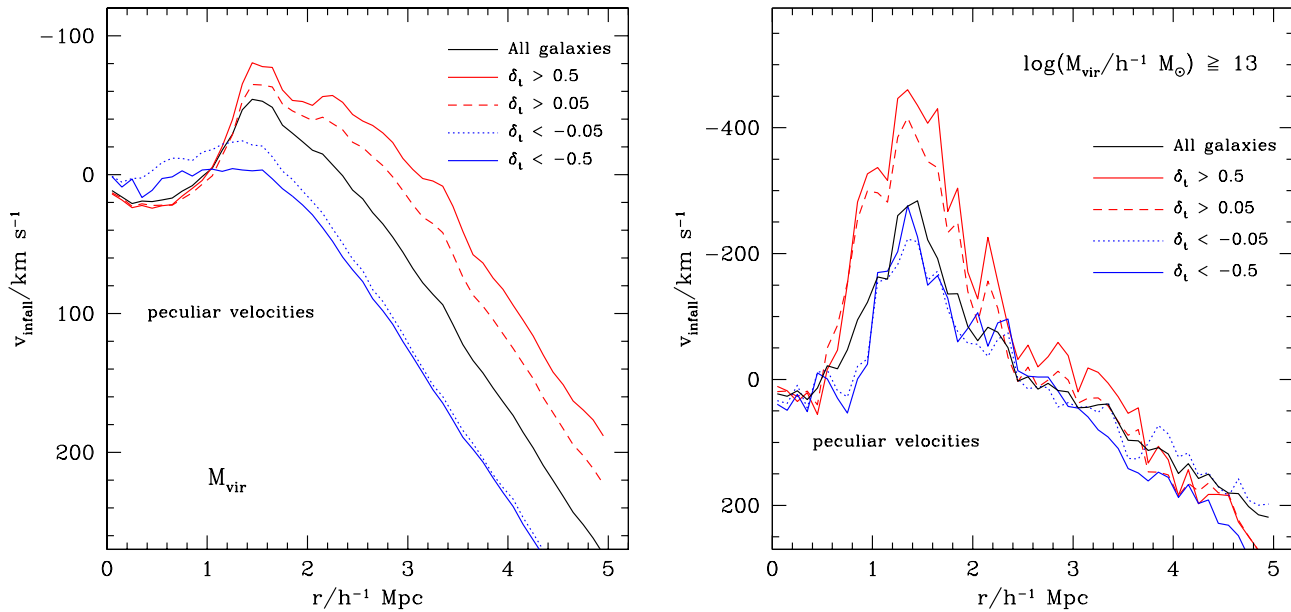
Figure 5. Radial velocity profiles around galaxies. The age parameter δ_t is given by the virial mass. The figure keys show the ranges of δ_t corresponding to the different symbols. The black solid line corresponds to the situation where the galaxies are not split according to their ages. *Left:* All haloes. In this case, the infall velocity for young galaxies (lower dotted and solid blue lines) does not have as clear a peak as that for old objects (upper solid and dashed red lines). *Right:* A subsample with high-mass objects, $M_{vir} \geqslant 10^{13} \ h^{-1} \ M_{\odot}$. The old and young galaxies (red and blue, respectively) have an akin profile, as both populations show a peak at $\sim 1.3 \ h^{-1}$ Mpc. This correlates with the smaller difference in clustering between old and young galaxies hosted by high-mass haloes.

values should depend on the initial density fluctuations as well as the clustering because, at large scales, the behaviour of haloes (and galaxies) is dominated by the collapse of these perturbations.

We calculate the radial velocity profile around galaxies, which can be expressed as

$$v_r(r) = v_{n_i}(r) - v_{c_i}, \qquad (13)$$

where v_{c_i} is the projected velocity of the central galaxy of the new halo along the direction between this galaxy and its ith neighboring galaxy located at a distance r, whose projected velocity along this direction is $v_{n_i}(r)$. The infall velocity at a distance r around galaxies is the average value of $v_r(r)$.

The v_{inf} profiles for young and old galaxies according to their virial masses are quite different (left-hand panel of Fig. 5). While the old galaxies (upper solid and dashed red lines) have a peak in their infall velocity distribution at $1.5 \ h^{-1}$ Mpc, the young population does not have a clear maximum (lower dotted and solid blue lines). The top of this distribution is rather flat around $1.3 \ h^{-1}$ Mpc. However, galaxies located in high mass haloes as those plotted in the top right panel of Fig. 4 should have similar velocity profiles, since they do not have a strong assembly bias. Their velocity profiles are shown in the right-hand panel of Figure 5. Both populations show similar infall velocity behaviours and a peak of the distribution at $\sim 1.3 \ h^{-1}$ Mpc.

The aim of the next section is to find the best values of the radius enclosing the mass of the density peak as a

function of both age and mass, in order to obtain similar velocity profiles and correlation functions for galaxies of very different ages but equal masses.

4.3 Parametrising a new overdensity peak height proxy

The previous sections have shown that a new proxy for the peak height could better characterise on average the assembly bias effect seen at large scales than the proxy given by the virial mass. Apart from the difference in clustering between populations of different ages but equal mass, the velocity profile could also be used to detect this bias.

We parametrise the radius of each galaxy as a function of both virial mass and δ_t. We then measure the masses inside spheres defined by this radius and calculate their relative ages with respect to this mass. Finally, a χ^2 statistics between the young and old populations of the differences between velocity profiles, $\chi^2_{v(r)}$, and correlation functions, $\chi^2_{\xi(r)}$, will be used to find the best parameter set that traces more accurately the assembly bias.

The radius for each galaxy is parametrised as

$$r = a \ \delta_t + b \ \log\left(\frac{M_{vir}}{M_{nl}}\right) , \qquad (14)$$

where M_{nl} is the non-linear mass defined by Seljak & Warren (2004, see Section 3.2), $\log(M_{nl}/h^{-1} \ M_{\odot}) = 13.38$ for our choice of cosmological parameters. The free parameters are a and b. The new peak height proxy will be the mass M enclosed within this radius. It is assumed that if r is smaller

Table 1. Best-fit parameters a and b from Equation (14). The last column shows the reduced χ^2 value.

a	b	$\chi^2_{v(r)}$	$\chi^2_{\xi(r)}$	χ^2
0.00	-0.07	7.80	23.68	31.48
0.20	-0.02	15.57	44.36	59.93

than the virial radius r_{vir} or if M is smaller than the virial mass, then $M = M_{vir}$.

Once the new mass contained in this radius and its δ_t are measured, infall velocities and correlation functions are calculated for three bins in mass corresponding to the first, second, and third terciles of the mass distribution. This selection produces results for low, medium, and high masses, respectively.

The χ^2 for the infall velocity field is calculated as

$$\chi^2_{v(r)} = \frac{1}{3} \sum_i^3 \left(\frac{1}{n_{dof}} \sum_r \frac{[v_{neg}(r) - v_{pos}(r)]^2}{\sigma^2_{v(r)}} \right)_i . \quad (15)$$

The χ^2 value for the ith mass bin is performed within the range $2.5 \leqslant r/h^{-1}$ Mpc $\leqslant 5$, since this interval corresponds to the two-halo regime; v_{neg} is the mean radial velocity around galaxies with $\delta_t < -0.05$ (young objects) and v_{pos} is this same quantity for $\delta_t > 0.05$ (old galaxies). The error is estimated as $\sigma^2_{v(r)} = \sigma^2_{v_{neg}} + \sigma^2_{v_{pos}}$, with the first term being the error for v_{neg} and the second term the error for v_{pos}, calculated as the error of the mean within the interval of interest. The symbol n_{dof} denotes the number of degrees of freedom. The value $\chi^2_{v(r)}$ is the average over the three mass bins.

Similarly, the reduced χ^2 for the correlation function statistics is defined as

$$\chi^2_{\xi(r)} = \frac{1}{3} \sum_i^3 \left(\frac{1}{n_{dof}} \sum_r \frac{[N_{neg}(r) - N_{pos}(r)]^2}{\sigma^2_{N(r)}} \right)_i , \quad (16)$$

and is calculated within the range $0.8 \leqslant r/h^{-1}$ Mpc $\leqslant 10$, mostly in the two-halo term; N_{neg} is the number of neighbours for young galaxies, whereas N_{pos} is the same quantity for old objects. The number of neighbours is defined as $N(r) = < N_t(r) > \xi(r) + < N_t(r) >$, where $< N_t(r) > = N_{pairs}(r)/N_{centres}$ is the mean number of tracers.[3] The error is $\sigma^2_{N(r)} = \sigma^2_{N_{neg}} + \sigma^2_{N_{pos}}$, where the first term is the error for N_{neg} and the second for N_{pos}, both calculated as the relative error of the number of neighbours. We choose this alternative to normalise the reduced χ^2 in order to avoid selecting parameters favoured by large uncertainties that can induce spuriously good fits. The value $\chi^2_{\xi(r)}$ is the average over the three mass bins.

The best-fit values are shown in Table 1. They were obtained by marginalising the reduced χ^2 for both the infall

velocity and correlation function statistics. Such marginalisation was done by integrating the likelihood

$$f(\chi) = e^{-(\chi - \chi_{min})^2/2} , \quad (17)$$

where χ_{min} is the minimum reduced χ value for a specific set of parameters. The final value is simply the sum of both results (last column in Table 1). We find that $f(\chi)$ has two maxima. The one corresponding to the best fit is that with $a = 0$ and $b = -0.07$. The fit corresponding to the second maximum in likelihood is that with $a = 0.2$ and $b = -0.02$. It is worth to mention that the reduced χ^2 value allows us to find the best parameters for a given sample and is not used with the aim of looking for the ideal parameters that would result in $\chi^2 \lesssim 1$, since Eq. (14) is only intended as an approximation to a more precise peak height proxy.

The infall velocity profiles and correlation functions for the parameters $a = 0$ and $b = -0.07$ are shown in Figures 6 and 7, respectively. Notice that in this case the size of the sphere in Equation (14) depends only on the halo mass, specifically $r = -0.07 \log(M_{vir}/M_{nl})$. The infall velocity profiles for old and young galaxies are very similar for each mass range. Furthermore, the correlation functions for these populations are remarkably similar at scales r > 1 h^{-1} Mpc for each mass bin, indicating that the assembly bias is not present using this redefinition of overdensity peak height. For the case $a = 0.2$ and $b = -0.02$, which depends on both the mass and age, we obtain similar correlation functions and infall velocity profiles, although with slight amplitude differences between populations of equal masses but different ages (not shown in Figs. 6 and 7 to improve the clarity of the figures).

Notice that with this new definition of peak height the one-halo terms of old and young objects of equal mass are comparable, a property which the virial mass was not able to produce.

Figure 8 shows the mass function for the parameters $a = 0$ and $b = -0.07$ as filled black circles, for $a = 0.2$ and $b = -0.02$ as open triangles, and for the virial mass as filled green squares. For comparison, the predicted mass functions from the extended Press-Schechter model (EPS) and from the Sheth, Mo, & Tormen (2001, SMT) model are shown as long-dashed and dot-dashed lines, respectively. At low masses, the $a = 0$, $b = -0.07$ distribution shows an unphysical behaviour, with very few objects at $M \sim 10^{10}$ h^{-1} M$_\odot$ and a bump at $\sim 10^{10.7}$ h^{-1} M$_\odot$. This means that most of the galaxies hosted by haloes in this range of virial mass (M_{vir}, green squares) changed their masses to $M \sim 10^{10.7}$ h^{-1} M$_\odot$ after using these parameters. However, the mass function changes only slightly with respect to that of the virial mass when using the second-best fit values $a = 0.2$ and $b = -0.02$ (open black triangles), which also reduces the assembly bias by introducing a dependence on the age. None of the two parametrisations change the mass function at $M \geqslant 10^{12}$ $h^{-1}M_\odot$, and therefore in this range their mass functions and the one resulting from the virial mass are all consistent with the SMT prediction. Therefore, we consider the second-best fit a better candidate since, by introducing a smaller variation in the mass, we find no assembly bias and a good agreement with SMT.

Figure 9 shows the distribution of r/r_{vir} for two differ-

---

[3] This relation comes from $\xi(r) = \frac{N(r) - <N_t(r)>}{<N_t(r)>}$. Therefore, if the distribution of neighbours is random, $\xi(r)$ would be equal to zero.
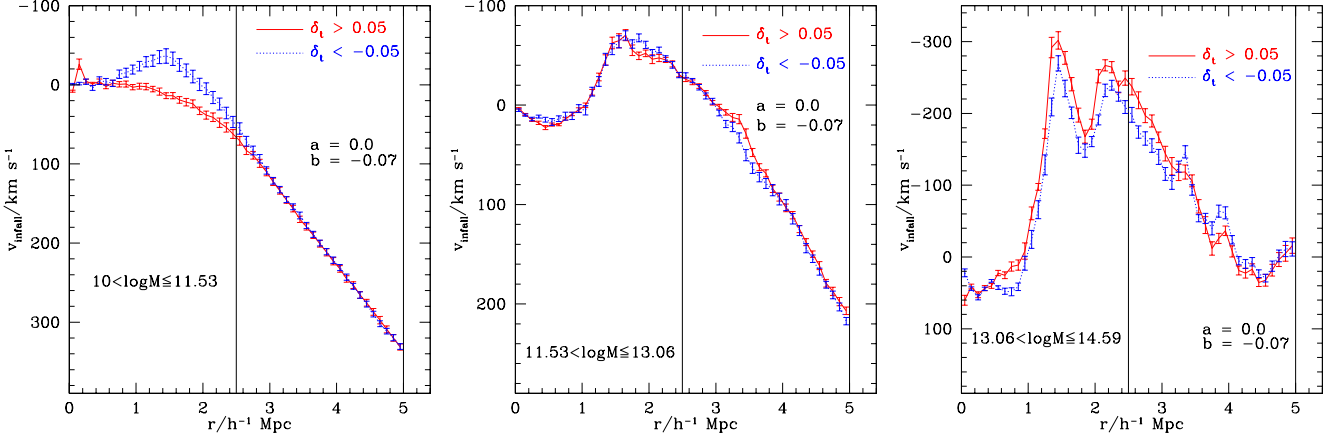
Figure 6. Infall velocity profiles for the best-fit parameters $a = 0$ and $b = -0.07$ (see Table 1). Solid lines in red are for old objects and dotted lines in blue are for young ones. Error bars were calculated using the jackknife method. Vertical lines mark the range in which the reduced $\chi^2_{v(r)}$ is calculated. The lower-mass bin is on the left-hand panel, whereas the more massive bin is on the right-hand panel. The mass M shown in the figure key is in units of h^{-1} M$_\odot$. Old and young objects show very similar infall velocity profiles, irrespective of the range in mass.
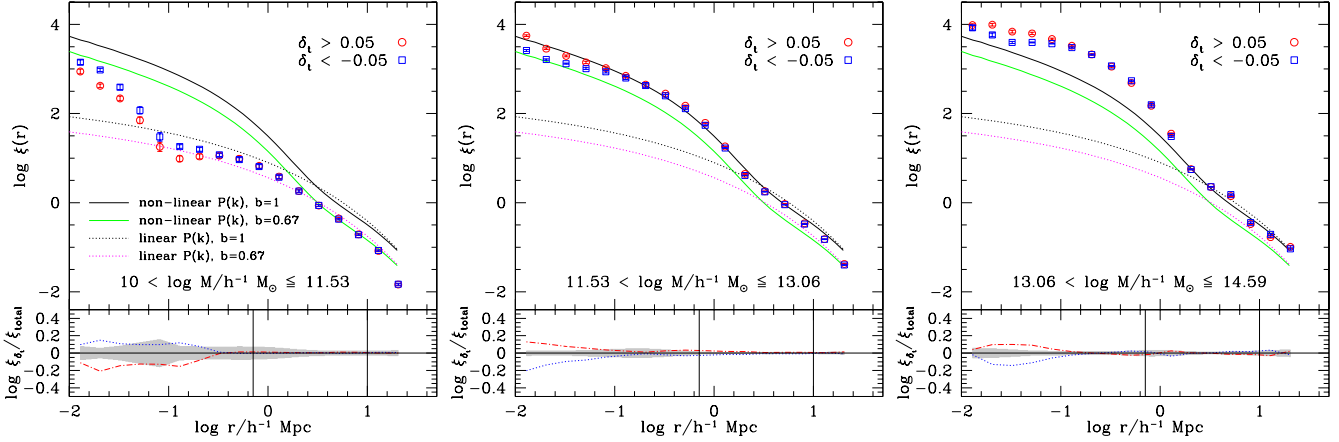
Figure 7. Correlation functions for the different mass bins indicated in each panel. Old (red circles) and young (blue squares) objects are selected by using the radius parametrisation in Equation (14) given by the best-fit parameters $a = 0$ and $b = -0.07$ (see Table 1). Error bars were calculated using the jackknife method. The lines repeated in each top box are obtained from the non-linear and linear power spectra, $P(k)$ (see Section 3.2). Lower boxes are as in Fig. 4. The vertical lines mark the range in which the reduced $\chi^2_{\xi(r)}$ is calculated. Note that the assembly bias is not present at large scales (r > 1 h^{-1} Mpc) in any of the mass bins presented. For smaller scales, the differences in the clustering amplitude between old and young populations are typically below a factor of two.

Table 2. Maximum and median radii, r_{max} and $< r >$, respectively, in physical units (h^{-1} kpc) from Equation (14), as given by the best-fit parameters in Table 1 for all objects and, also, split among the old and young populations of galaxies. The ranges in virial mass are those shown in Fig. 9.

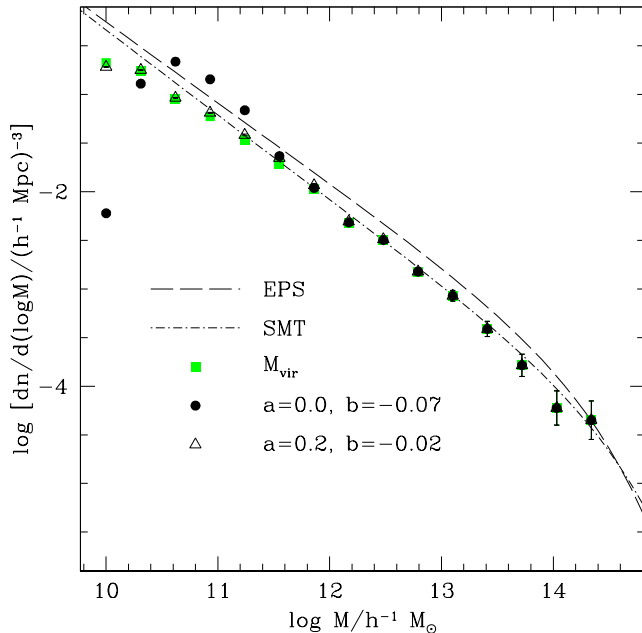| best-fit params.	ages	r_{max}	$< r >$	r_{max}	$< r >$
		$\log(M_{vir}/h^{-1}M_\odot)$ =	10.3 - 10.7	$\log(M_{vir}/h^{-1}M_\odot)$ =	10.8 - 11.4
$a = 0.0,\ b = -0.07$	all	215.5	205.3	180.6	165.4
	old	215.5	204.2	180.6	166.3
	young	215.5	207.5	180.6	163.1
$a = 0.2,\ b = -0.02$	all	415.9	55.9	445.2	86.6
	old	415.9	101.8	445.2	123
	young	383.5	51.1	407.8	76.6

Figure 8. Mass function obtained from using the virial mass (M_{vir}, filled green squares) and the new masses from the best-fit parameters $a = 0$, $b = -0.07$ (filled black circles) and $a = 0.2$, $b = -0.02$ (open black triangles). Error bars correspond to the Poisson error. For comparison, we plot the mass functions from the EPS (long-dashed line) and the SMT (dot-dashed line) models. The best agreement with the SMT mass function is shown by the results from virial masses and those from the second-best set of parameters $a = 0.2$ and $b = -0.02$.

ent bins in *virial* mass for the two sets of best-fit parameters in Table 1. Both panels show that most of the galaxies keep their original halo masses, M_{vir}, when using the best-fit parameters $a = 0.2$ and $b = -0.02$ (solid lines). For the lower-mass bin (left panel), these galaxies have a median value of $r = r_{vir}$. For the case $a = 0$ and $b = -0.07$ (dashed lines), they have a median value of $r \sim 4\,r_{vir}$. The maximum and median radii (in units of r_{vir}) and, also, the number of objects which change their mass, decrease for higher virial masses. Table 2 shows these radii in units of kpc. All the galaxies with $M_{vir} \geqslant 6 \times 10^{12}\ h^{-1} M_\odot$ conserved their virial masses, i.e. $M = M_{vir}$, in both cases. This means that some objects which were initially considered as those with low peak heights, as given by their virial mass, are now associated to regions with higher overdensities, particularly for low virial masses.

5   PROPERTIES OF THE NEW PEAKS

We have presented a new proxy for the peak height that can account for the assembly bias at large scales (Section 4). In some cases this model considers the mass enclosed by radii greater than the virial radius, inside which one could be including other haloes. In order to see differences between the old and young populations and how these could affect the statistics for $\xi(r)$ and $v_{inf}(r)$, Figure 10 shows the number of haloes inside each new peak height (when $r > r_{vir}$), excluding the central galaxy, as a function of the ratio between

their virial mass and the virial mass of the central galaxy, M_{vir_c}, for the mass ranges and parameters shown in Figure 9. As can be seen from both panels, there is a trend where the number of haloes contained in spheres of size r around young galaxies (blue) is lower than that for spheres around old objects (red), the effect being stronger for higher virial masses (right panel). Therefore, the peak for an old galaxy, after taking into account the parametrisation of the radius from Equation (14), adds more haloes and mass than for a young object. Furthermore, we can see that the higher the virial mass, the lower is the influence of other haloes in defining the new peak height for galaxies.

Another interesting result is that, for the parameters $a = 0.2$ and $b = -0.02$, both old (solid red lines) and young (dotted blue lines) populations tend to add massive peaks, as can be seen from the left panel of Figure 10, which shows that the maximum ratio where the distribution is non-zero is $\log(M_{vir}/M_{vir\_c}) \sim 4$, but the minimum is $\log(M_{vir}/M_{vir\_c}) \sim -0.6$ and 0.4 for the old and young galaxies, respectively. For the case $a = 0$ and $b = -0.07$, young objects (long-dashed blue curves) show a peak around $M_{vir} = 0.6 \times M_{vir\_c}$, but they include a broad range of more massive haloes. Old objects (dashed red curves) are characterised by this same behaviour and additionally show a peak at $\log(M_{vir}/M_{vir\_c}) \sim 1.7$. These results indicate that old, low-mass objects are surrounded preferentially by high-mass haloes. The latter is consistent with recent results which show that old, low-mass galaxies suffer truncation of matter by nearby massive haloes (Wang et al. 2007; Dalal et al. 2008; Hahn et al. 2009). However, our results also indicate that there is a population of low-mass objects which are surrounded by smaller masses. In particular, for the $a = 0.2$ and $b = -0.02$ case, this is only seen for old objects, regardless of their M_{vir_c}. It is possible that galaxies with low and high M_{vir}/M_{vir_c} ratios correspond to different aspects of the assembly bias phenomenology. This, along with studies of the prevalence of this bias by varying the concentration, number of satellites, triaxiality, spin, and other halo parameters, are the focus of a forthcoming paper (Lacerna et al. in preparation).

6   CONCLUSIONS

We have presented a new approach to estimate the overdensity peak height with the aim to understand the assembly bias effect. This is a relevant issue that could affect the ability of the next generation of galaxy surveys to infer accurate cosmological parameters. Our method consisted in redefining the overdensity that characterises each galaxy using the information of its virial mass and the relative age, δ_t; this new definition is proposed as a better alternative than the virial mass. Wang et al. (2007) pointed out that old, low-mass haloes at $z = 0$ are associated to higher overdensities in the initial conditions, compared to what would be expected from their final virial masses. Instead of searching for the overdensity at high redshifts, we try to obtain a measure of the present-day peak height, which in turn can be tested using large, $z = 0$ surveys. In order to do this, we measure the assembly bias amplitude using two estimators, the two-point correlation function and the infall velocity profile. We find that when using the mass inside spheres of radius r
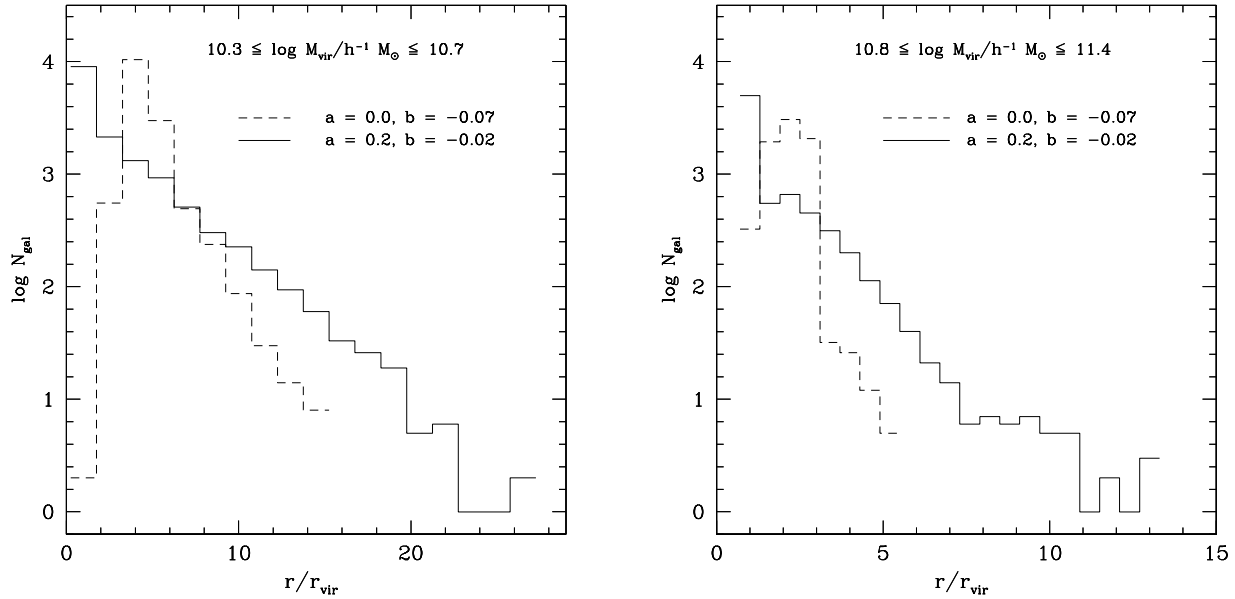
Figure 9. Distribution of r/r_{vir} for different ranges of virial mass M_{vir} for the best-fit parameters in Table 1. For higher values of M_{vir}, fewer objects change their halo masses. All the galaxies with $\log(M_{vir}/h^{-1}\ M_\odot) \geqslant 12.8$ conserved their virial masses (i.e. $r = r_{vir}$).
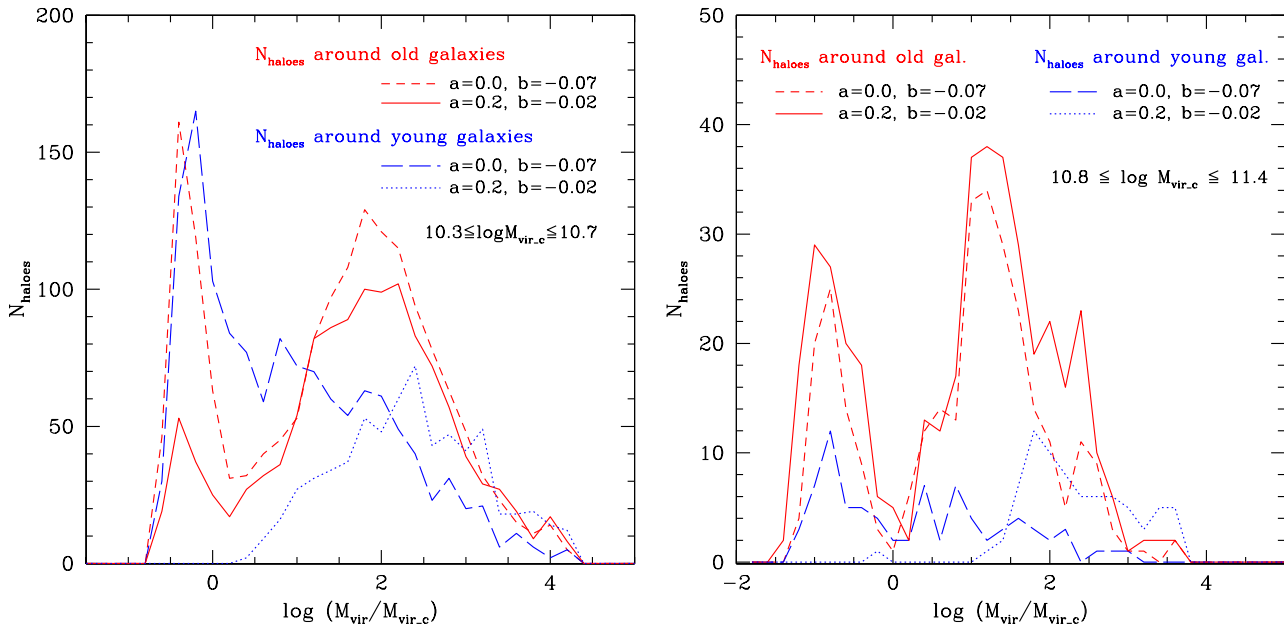

Figure 10. Number of haloes inside radius r (Eq. 14) given by the best-fit parameters in Table 1: $a = 0$, $b = -0.07$ (dashed and long-dashed curves around old and young galaxies, respectively) and $a = 0.2$, $b = -0.02$ (solid and dotted curves around old and young galaxies, respectively). The results are plotted as a function of the virial mass normalised by the virial mass of the central galaxy, M_{vir_c}. The mass range is shown in each panel, where M_{vir_c} is in units of $h^{-1}\ M_\odot$.

from Equation (14) with the parameters in Table 1, galaxies do not show significant differences in the two-halo regime for objects of a given mass range but different age. Furthermore, the dependence on the age is reduced in the one-halo term as well; the biggest difference is of a factor of two for the lowest mass bin at a separation of $r \sim 150\ h^{-1}$ kpc, which—when using virial masses—becomes a difference of

two orders of magnitude in the clustering amplitude at the same scale.

The best-fit parameters $a = 0$ and $b = -0.07$ imply that the relative age is not strictly necessary (see Equation 14) to find a peak height that includes the mass that has not collapsed completely onto haloes yet, and at the same time traces the assembly bias. We found that the best parameters

are those that yield median sphere radii in the range of 1 - 4 r_{vir}. Clearly, environmental effects out to these distances are playing the main role in shaping the two-halo term, as shown in Fig. 9. It is worth to point out that only low-mass objects, with $M_{vir} \leqslant 6 \times 10^{12} \ h^{-1} M_\odot$, are subject to a change in their peak heights, which coincides with the mass limit for assembly bias found by several authors (e.g. Gao et al. 2005). This is also the case for our second-best fitting parameters, $a = 0.2$ and $b = -0.02$, which introduce a dependence of the peak height on the age, and help trace the assembly bias while at the same time produce final masses that are in excellent agreement with the SMT mass function. Therefore, this option is the preferred one to obtain a proxy for the peak height which is not subject to the assembly bias effect.

Neighbouring massive haloes that are typically at distances out to 4 r_{vir} (see Figs. 9 and 10) are probably responsible for these effects. These could disrupt the normal growth of small objects and, therefore, affect their ages. However, we also find a population of haloes which, with the new definition, includes nearby low-mass haloes, particularly for old objects.

To summarise, we stress the apparent fact that particularly for low-mass objects, the *virial* mass is not an adequate proxy for peak height in the standard EPS picture, because equal virial mass objects can actually belong to initial density peaks of very different amplitude, as evidenced in the large differences shown in the 2-halo regime by statistics such as the correlation function and infall velocities. It is necessary to include a more global environmental component, i.e. the mass of the region that effectively characterises the peak height. When the latter is taken into account, we obtain the general prescription where the bias responds to the height of the mass peak alone at large scales. Further work is required in order to confirm that this proposed parametrisation of the peak height is enough to account for other variations of clustering of equal mass haloes with different properties such as concentration, spin, etc. The next papers in this series will study this, along with an application of this method to large surveys.

REFERENCES

Balogh M., et al., 2004, MNRAS, 348, 1355
Baugh C. M., et al., 2005, MNRAS, 356, 1191
Berlind A., et al., 2003, ApJ, 593, 1
Bett P., et al., 2007, MNRAS, 376, 215
Bond J. R., Cole S., Efstathiou G., Kaiser N., 1991, ApJ, 379, 440
Bornancini C., Padilla N., Lambas D. G., De Breuck C., 2006, MNRAS, 368, 619
Boylan-Kolchin M., Springel V., White S. D. M., Jenkins A., Lemson G., 2009, MNRAS, 398, 1150
Ceccarelli L., Padilla N., Lambas D. G., 2008, MNRAS, 390, L9
Cooper M. C., Gallazzi A., Newman J. A., Yan R., 2010, MNRAS, 402, 1942
Croton D. J., Gao L., White S. D. M., 2007, MNRAS, 374, 1303
Dalal N., White M., Bond J. R., Shirokov A., 2008, ApJ, 687, 12
Faltenbacher A., White S. D. M., 2010, ApJ, 708, 469
Gallazzi A., Charlot S., Brinchmann J., White S. D. M., Tremonti C. A., 2005, MNRAS, 362, 41
Gao L., Springel V., White S. D. M., 2005, MNRAS, 363, 66
Gao L., White S. D. M., 2007, MNRAS, 377, L5
Gomez P. L., et al., 2003, ApJ, 584, 210
Gonzalez R. E., Padilla N., 2009, MNRAS, 397, 1498
Gunn J. E., Gott J. R., 1972, ApJ, 176, 1
Hahn O., Porciani C., Dekel A., Carollo C. M., 2009, MNRAS, 398, 1742
Hester J. A., Tasitsiomi A., 2010, ApJ, 715, 342
Kauffmann G., Nusser A., Steinmetz M., 1997, MNRAS, 286, 795
Kauffmann G., et al., 2003, MNRAS, 341, 33
Lacey C., Cole S., 1993, MNRAS, 262, 627
Lagos C., Cora S. A., Padilla N., 2008, MNRAS, 388, 587
Lagos C., Padilla N., Cora S., 2009, MNRAS, 395, 625
Li Y., Mo H. J., Gao L., 2008, MNRAS, 389, 1419
Ludlow A. D., et al., 2009, ApJ, 692, 931
Mo H. J., White S. D. M., 1996, MNRAS, 282, 347
Padilla N. D., Lambas D. G., Gonzalez R., 2010, MNRAS, tmp, 1417
Percival W. J., Scott D., Peacock J. A., Dunlop J., 2003, MNRAS, 338, L31
Press W. H., Schechter P., 1974, ApJ, 187, 425
Seljak U., Warren M. S., 2004, MNRAS, 355, 129
Sheth R. K., Mo H. J., Tormen G., 2001, MNRAS, 323, 1
Smith R. E., et al., 2003, MNRAS, 341, 1311
Springel et al., 2005, Nature, 435, 629
Yang, X., Mo, H. J., van den Bosch, F. C., 2003, MNRAS, 339, 1057
Wang H., Mo H. J., Jing Y. P., 2007, MNRAS, 375, 633
Wang H., Mo H. J., Jing Y. P., 2009, MNRAS, 396, 2249
Wang Y., Yang X., Mo H. J., van den Bosch F., Weinmann S., Chu Y., 2008, ApJ, 687, 919
Wechsler R. H., Zentner A. R., Bullock J. S., Kravtsov A. V., Allgood B., 2006, ApJ, 652, 71
Wu H., Rozo E., Wechsler R. H., 2008, ApJ, 688, 729
Zapata T., Perez J., Padilla N., Tissera P., 2009, MNRAS, 394, 2229
Zentner A. R., 2007, IJMPD, 16, 763
Zhu G., et al., 2006, ApJ, 639, L5